Data report: Rb and Cs concentration analyses of pore fluids from offshore Osa Peninsula, Costa Rica, IODP Expedition 344[1]

Miriam Kastner[2]

Chapter contents

[1] Kastner, M., 2017. Data report: Rb and Cs concentration analyses of pore fluids from offshore Osa Peninsula, Costa Rica, IODP Expedition 344. *In* Harris, R.N., Sakaguchi, A., Petronotis, K., and the Expedition 344 Scientists, *Proceedings of the Integrated Ocean Drilling Program,* 344: College Station, TX (Integrated Ocean Drilling Program). doi:10.2204/iodp.proc.344.207.2017
[2] Scripps Institution of Oceanography, La Jolla, CA 92037, USA.
mkastner@ucsd.edu

Abstract

The Rb and Cs concentrations of pore fluids recovered during Integrated Ocean Drilling Program (IODP) Costa Rica Seismogenesis Project Expedition 344 are reported. Five sites were drilled during IODP Expedition 344, three in the overriding plate (Sites U1380, U1413, U1412) and two on the incoming Cocos plate (Sites U1381, U1414). One of the sites drilled in the overriding plate, Site U1380, is a complementary site to the adjacent Site U1378 drilled during expedition 334.

The Rb and Cs systematics were analyzed to unravel the behavior of the highly incompatible alkali metal elements at the different sites in order to better understand the fractionation between them and K during fluid-rock reactions at greater depths in forearc basins.

The pore fluids at the sites drilled on the upper plate suggest an important role of ash (or tephra) alteration for K concentrations; however, this role is less apparent for Rb and particularly for Cs concentrations. At the three overriding plate sites drilled, communication with a deeper Cs-enriched fluid is observed, suggesting that the most incompatible alkali metal element, Cs, is not involved in the overriding plate sediment diagenetic reactions and hence is expelled into the fluid phase that is circulating at great depths. Some of the Rb is, however, involved in certain clay and possibly zeolite diagenetic reactions but not in carbonate or silica recrystallization reactions. At the two incoming plate sites cored during this expedition, Sites U1381 and U1414, the pore fluids are enriched in both Rb and Cs, as discussed below.

Introduction

The study region of the Costa Rica Seismogenesis Project (CRISP), located offshore the Osa Peninsula, is part of an extensive erosional subduction zone, spanning from Guatemala to Costa Rica (Ranero and von Huene, 2000; Ranero et al., 2000; Vannucchi et al., 2004). The CRISP drilling project was aimed at understanding the processes that control fault zone behavior during earthquake nucleation and rupture propagation at erosional subduction zones. This region is characterized by low sediment supply, fast convergence rate, abundant seismicity, and change in subducting plate relief along strike (see the **Expedition 344 summary** chapter [Harris et al., 2013a]). Arcward of the trench, the lower slope

doi:10.2204/iodp.proc.344.207.2017

consists of a 10–12 km wide frontal prism, where a modern sediment apron overlies older sediment that may have been deposited in a forearc basin setting (Ross et al., 2015). Five sites were drilled, three on the overriding and two on the incoming plates (Fig. F1).

Pore fluids were subsampled and analyzed for Cl, K, Rb, and Cs concentrations at the five sites drilled during Expedition 344, and the results are reported below (Table T1; Figs. F2, F3, F4, F5, F6).

Drill sites

Two of the sites that were drilled on the overriding plate sampled the upper and middle slope regions, and at Site U1412 the prism toe was drilled; the other two sites were drilled on the incoming Cocos plate (Fig. F1). (For complete descriptions of the drilling results see the **Expedition 344 summary** chapter [Harris et al., 2013a]).

Overriding plate sites

Site U1380 is a complementary site to the adjacent Site U1378, drilled during Expedition 334 to ~480 meters below seafloor (mbsf) and abandoned because of hole instability. The hole was washed to ~450 mbsf and drilled to ~800 mbsf; however, pore fluids were only recovered between ~450 and ~600 mbsf. At greater depths the sediments were cemented and no porefluids were recovered. Site U1380 was drilled to investigate the deeper portions of the upper slope sequence and underlying wedge sediments. The sedimentary succession recovered from the wedge consists of alternating terrestrial turbiditic upper slope to shelf sequences, with some deltaic-derived sediment.

Site U1413 was also drilled in the middle slope region along a 3-D seismic line (Bangs et al., 2013). Three lithostratigraphic units were distinguished in the sediment section of Site U1413 (see the **Upper slope Site U1413** chapter [Harris et al., 2013e]).

The frontal sedimentary prism at the base of the slope was drilled at Site U1412. The primary goal at this site was to penetrate the décollement and to investigate the fluid flow regime within the underthrust sediments as well as within the oceanic crust. Three units were distinguished in the sedimentary section; unfortunately, due to hole instability, the décollement, underthrust sediment, and basement were not sampled at this site.

Incoming plate sites

Two sites were drilled on the subducting aseismic Cocos Ridge in order to understand seismogenic processes in subduction zones. The incoming sediment thickness at Site U1381 is just <100 m, and the site is located higher on the Cocos Ridge. The upper 50 m at this site consists of predominantly monotonous sequences of silty clay to clay underlain by a more pelagic sequence with abundant biogenic sediment. The contact between the basement and the overlying sediment was recovered at ~95 mbsf in Hole U1381B and at ~104 mbsf in Hole U1381C.

The sediment thickness at Site U1414 is ~380 m; the sediment section consists of pelagic/hemipelagic silty clay to clay in the upper section with increasing nannofossil-rich calcareous ooze at greater depth plus interspersed tephra layers, mostly missing at Site U1381. Below ~345 mbsf the sediments were too indurated for pore fluid extraction (see the **Input Site U1414** chapter [Harris et al., 2013b]).

Analytical methods

Pore fluid was collected from whole-round cores that were cut on the catwalk immediately after recovery, capped, and taken to the laboratory for processing using a titanium squeezer (Manheim and Sayles, 1974). Gauge pressures up to 30 MPa were applied using a hydraulic press to extract pore fluids. The extracted pore fluid was passed through a prewashed Whatman No. 1 filter fitted above a titanium screen, filtered through a 0.2 µm Gelman polysulfone disposable filter, and subsequently extruded into a precleaned (10% HCl), 60 mL plastic syringe attached to the bottom of the squeezer assembly. Details of this procedure are given in the **Methods** chapter (Harris et al., 2013d).

High-precision chloride concentrations were acquired on board using a Metrohm 785 DMP autotitrator and silver nitrate ($AgNO_3$). International Association for the Physical Sciences of the Oceans (IAPSO) seawater was used as the standard (see the **Methods** chapter [Harris et al., 2013d]). The Cl concentrations were reanalyzed on shore at Scripps Institution of Oceanography by titration with $AgNO_3$ (1% precision).

Rubidium and cesium concentrations in the pore fluids were analyzed using a Thermo Scientific iCAP Q inductively coupled plasma–mass spectrometer (ICP-MS) in the Scripps Isotope Geochemistry Lab (SIGL) at Scripps Institute of Oceanography. Concentrations were determined using a calibration curve methodology.

A primary standard of 500 ppb Rb and 5 ppb Cs in 1% HNO_3 was diluted to 50%, 25%, 10%, 5%, and 1% concentrations with 1% 15 M ultra-pure (optima) HNO_3. For analysis, a 100 uL aliquot of 500 ppb indium standard was added to an empty, acid

cleaned analysis vial. A 300 uL aliquot of this standard and 4.7 mL of 1% HNO_3 were added to the analysis vial. Additionally, 150 uL of a 560 mM NaCl solution was added to the analysis vial to account for matrix suppression of the plasma ionization efficiency. In total, the standard was diluted to 5.7% of its original concentration. The 25% standard was diluted as above and analyzed after every five samples throughout the analysis series to determine precision of the results. A blank solution was analyzed before and after the sample set was analyzed to determine residual carryover of any elements throughout the analysis.

Prior to sample analysis, the ICP-MS was calibrated using an internal indium (In) standard to maximize the intensity of the elements to be analyzed. Instrumental drift was corrected online by normalization of the intensity of the analyte with the intensity of the indium standard. A secondary drift correction was applied offline on each measured concentration using a 1.0 ppb indium calibration standard that was analyzed after every four samples.

Before diluting samples, a 100 uL aliquot of 500 ppb In standard was added to empty, acid cleaned analysis vials. Then a 300 uL aliquot of the sample and 4.7 mL of 1% HNO_3 were added to the analysis vial (diluting the sample to 5.7% of its original concentration) based on previous determination of the detection limits; previous attempts of 150 uL sample with 4.85 mL 1% HNO_3 proved to have low precision. There were 50 samples tested in total, 12 of which were duplicates to ensure conformity of results within samples.

Results and discussion

The data are listed in Table T1. Figures F2, F3, F4, F5, and F6 show the K, Rb, and Cs concentration-depth profiles and their cross-element mixing plots.

Overriding plate sites

Site U1380

Site U1380 was drilled to investigate the deeper portions of the upper slope sequence and the underlying wedge sediments. The sedimentary succession recovered from the framework wedge consists of alternating terrestrial upper slope turbidites and shelf sequence, with some input from deltaic sediments. As mentioned above, this site is complementary to the adjacent Site U1378 drilled during expedition 334 to ~480 mbsf; therefore, Site U1380 was washed to ~450 mbsf and drilled to ~800 mbsf. Because of cementation at >600 mbsf, pore fluids were only recovered between ~450 and ~600 mbsf.

Chloride concentrations of the pore fluids are fresher than modern seawater by 30%–36%, suggesting communication with a fluid that migrated from a deeper source where the temperature is >60°C, high enough to support clay dehydration reactions (e.g., Perry and Hower, 1970; Bekins et al., 1994, and references therein). The in situ temperature at the depth range of the Site U1380 pore fluid samples is just 25°–32°C, lower than the required temperature for the smectite to illite (S/I) transformation reaction. K concentrations as well decrease with depth but to a greater extent than the observed Cl dilution (Table T1), indicating that, in addition to dilution, K is also involved in fluid-mineral reactions, most likely in the S/I transformation reaction. The concentration-depth profile of Rb, normalized to Cl, mimics that of K concentration (Fig. F2). The Cs concentration profile (also normalized to Cl) is also similar to the K and Rb profiles to ~540 mbsf; at >540 mbsf, however, Cs concentration abruptly increases. Based on just one datum point it is impossible to conclude if this increase is a sample handling problem or a real datum point that suggests an in situ diagenetic reaction that releases Cs.

Site U1413

Site U1413 was also drilled in the middle slope region along a 3-D seismic line (Bangs et al., 2013). The objectives were to determine the nature, composition, and physical properties of the slope sediment and to constrain the fluid regime of the slope sediments. The upper ~150 mbsf is a slump. Three lithostratigraphic units were distinguished in the sediment section. At this site the Cl concentrations somewhat decrease with depth below the slump, suggesting minor lateral flow of fresher fluid in the more sandy horizons at ~500 mbsf. Several tephra layers were recovered at the top of the section and between 135 and 180 mbsf.

Similar to Cl concentrations K concentrations also gradually decrease with depth and could be related to the decrease in the Cl concentration; some of the decrease in K concentration could as well be caused by tephra alteration to illite/smectite or to zeolites.

The Rb depth-concentration profile (normalized to Cl) (Fig. F3) is very similar to that of K; Rb and K may be involved in the same diagenetic reactions. Cesium concentrations, however, remain constant with depth except for an increase at ~500 mbsf, which is very similar to the increase in Cs observed at Site U1380 at a similar depth, where some sand layers are present. The cause of this increase is as yet unclear, and could be caused by some lateral flow of a fluid enriched in Cs.

Site U1412

At Site U1412, drilled on the prism toe, borehole instability precluded sampling the décollement and recovering the underthrust sediment and igneous basement. Sample recovery was very poor especially in the deeper parts of the section below the bottom simulating reflection (BSR) at ~200 mbsf. Neither Cl nor K concentrations vary significantly with depth except for the artifact caused by localized gas hydrate dissociation in some upper section horizons. The Rb concentration-depth profile and the K/Rb mixing plot (Fig. **F4**), although similar above the BSR, indicate some increase in Rb but not in K concentration at depth; carbonate recrystallization would exclude Rb but not K. The Cs profile deviates even more from the K concentration-depth profile—Cs concentrations gradually increase with depth from ~100 mbsf, suggesting diffusional communication with a deeper Cs-enriched fluid.

All the above overriding plate sites show communication with a deeper Cs-enriched fluid, suggesting that the most incompatible element—Cs—is not involved in any of the most important overriding plate sediment diagenetic reactions; hence, Cs is being expelled into the fluid phase that is circulating at greater depths. At Site U1412, the deepest pore fluid samples analyzed closest to the décollement, are also enriched in Rb, possibly suggesting communication with the underthrust section, which may be enriched in both Rb and Cs.

Incoming plate sites

The incoming plate Sites U1381 and U1414 were cored to characterize the nature of the sediments and oceanic crust entering the seismogenic zone.

Site U1381

Although cored during Expedition 334, Site U1381 was cored again during Expedition 344 in order to acquire higher-resolution data on the incoming plate. No significant variations in the Cl concentrations with depth are observed. The K concentrations, however, decrease with depth, most likely caused by ash alteration to clay minerals and possibly to zeolites. Both Rb and Cs concentrations decrease in the uppermost part of the section (Fig. **F5**); the ash alteration reactions to clay minerals and particularly possibly to zeolites could be responsible for the observed uptake of Rb. The cause of the decrease in Cs concentration is as yet unclear but could be caused by lateral fluid flow.

Several of the geochemical profiles at this site, especially of Sr and sulfate concentrations acquired shipboard, suggest that the pore fluids in the deeper sediment section at this site are influenced by diffusional communication with a fluid in the igneous basement (see the **Input Site U1381** chapter [Harris et al., 2013c]), altered seawater. This was also observed, for example, at Sites U1039 and U1253 drilled offshore Nicoya Peninsula during ODP Legs 170 and 205, respectively (Silver et al., 2000; Morris, Villinger, Klaus, et al., 2003). Both Rb and Cs concentrations increase at greater depths at Site U1381. This suggests that the basement fluid is enriched in both Rb and Cs.

Site U1414

Site U1414 Cl concentrations do not vary with depth. Similar to Site U1381, K concentrations decrease with depth; some of the tephra alteration to clay minerals (and possibly zeolites) must be responsible for this observation. The Rb and Cs depth-concentration profiles (Fig. **F6**) suggest some uptake in the uppermost ~100 m; below, however, the concentrations increase with depth and show a sharp increase at ~300 mbsf, at the boundary between two lithologic units (Unit II/III boundary; Harris et al., 2013). A seismic reflector is observed at this depth, where carbonate cementation increases abruptly. No pore fluids could be recovered from the lowermost ~65 m of the sediment section, which is characterized by a sequence of lithified, calcareous, and siliceous cemented silt- and sandstone. Large increases in the concentrations of both Rb and Cs in the deepest pore fluids recovered, above the recrystallized section, indicates that during intense recrystallization and cementation of calcareous and siliceous oozes these two incompatible elements are being expelled into the fluid phase; hence, they could be used as a proxy for fluid flow at greater depths in forearcs.

The sediment cemented basal section prevents communication with the basement fluid observed at Site U1381.

Acknowledgments

This research used samples and data provided by the Integrated Ocean Drilling Program (IODP). The efforts of the *JOIDES Resolution* shipboard and drilling personnel and of the scientific party of IODP Expedition 344 are greatly appreciated. I also thank Ms. Gretchen Robertson for the Cl, Rb, and Cs analyses at SIO and Graham Boud for helping with the figures and table. This research was partially funded by a USSSP postcruise research award to Miriam Kastner.

References

Bangs, N.L., McIntosh, K.D., Silver, E.A., Kluesner, J., and Ranero, C.R., 2013. Structural controls on the hydrogeology of the Costa Rica subduction thrust NW of the Osa Peninsula [presented at the 2013 American Geophysical Union Fall Meeting, San Francisco, CA, 9–13 December 2013]. (Abstract T51I-01) **http://abstractsearch.agu.org/meetings/2013/FM/T51I-01.html**

Bekins, B., McCaffrey, A.M., and Dreiss, S.J., 1994. Influence of kinetics on the smectite to illite transition in the Barbados accretionary prism. *Journal of Geophysical Research: Solid Earth,* 99(B9):18147–18158. **https://doi.org/10.1029/94JB01187**

Expedition 334 Scientists, 2012. Expedition 334 summary. *In* Vannucchi, P., Ujiie, K., Stroncik, N., and the Expedition 334 Scientists, *Proc. IODP, 334:* Tokyo (Integrated Ocean Drilling Program Management International, Inc.). **doi:10.2204/iodp.proc.334.101.2012**

Harris, R.N., Sakaguchi, A., Petronotis, K., Baxter, A.T., Berg, R., Burkett, A., Charpentier, D., Choi, J., Diz Ferreiro, P., Hamahashi, M., Hashimoto, Y., Heydolph, K., Jovane, L., Kastner, M., Kurz, W., Kutterolf, S.O., Li, Y., Malinverno, A., Martin, K.M., Millan, C., Nascimento, D.B., Saito, S., Sandoval Gutierrez, M.I., Screaton, E.J., Smith-Duque, C.E., Solomon, E.A., Straub, S.M., Tanikawa, W., Torres, M.E., Uchimura, H., Vannucchi, P., Yamamoto, Y., Yan, Q., and Zhao, X., 2013a. Expedition 344 summary. *In* Harris, R.N., Sakaguchi, A., Petronotis, K., and the Expedition 344 Scientists, *Proceedings of the Integrated Ocean Drilling Program,* 344: College Station, TX (Integrated Ocean Drilling Program). **https://doi.org/10.2204/iodp.proc.344.101.2013**

Harris, R.N., Sakaguchi, A., Petronotis, K., Baxter, A.T., Berg, R., Burkett, A., Charpentier, D., Choi, J., Diz Ferreiro, P., Hamahashi, M., Hashimoto, Y., Heydolph, K., Jovane, L., Kastner, M., Kurz, W., Kutterolf, S.O., Li, Y., Malinverno, A., Martin, K.M., Millan, C., Nascimento, D.B., Saito, S., Sandoval Gutierrez, M.I., Screaton, E.J., Smith-Duque, C.E., Solomon, E.A., Straub, S.M., Tanikawa, W., Torres, M.E., Uchimura, H., Vannucchi, P., Yamamoto, Y., Yan, Q., and Zhao, X., 2013b. Input Site U1414. *In* Harris, R.N., Sakaguchi, A., Petronotis, K., and the Expedition 344 Scientists, *Proceedings of the Integrated Ocean Drilling Program,* 344: College Station, TX (Integrated Ocean Drilling Program). **https://doi.org/10.2204/iodp.proc.344.104.2013**

Harris, R.N., Sakaguchi, A., Petronotis, K., Baxter, A.T., Berg, R., Burkett, A., Charpentier, D., Choi, J., Diz Ferreiro, P., Hamahashi, M., Hashimoto, Y., Heydolph, K., Jovane, L., Kastner, M., Kurz, W., Kutterolf, S.O., Li, Y., Malinverno, A., Martin, K.M., Millan, C., Nascimento, D.B., Saito, S., Sandoval Gutierrez, M.I., Screaton, E.J., Smith-Duque, C.E., Solomon, E.A., Straub, S.M., Tanikawa, W., Torres, M.E., Uchimura, H., Vannucchi, P., Yamamoto, Y., Yan, Q., and Zhao, X., 2013c. Input Site U1381. *In* Harris, R.N., Sakaguchi, A., Petronotis, K., and the Expedition 344 Scientists, *Proceedings of the Integrated Ocean Drilling Program,* 344: College Station, TX (Integrated Ocean Drilling Program). **https://doi.org/10.2204/iodp.proc.344.103.2013**

Harris, R.N., Sakaguchi, A., Petronotis, K., Baxter, A.T., Berg, R., Burkett, A., Charpentier, D., Choi, J., Diz Ferreiro, P., Hamahashi, M., Hashimoto, Y., Heydolph, K., Jovane, L., Kastner, M., Kurz, W., Kutterolf, S.O., Li, Y., Malinverno, A., Martin, K.M., Millan, C., Nascimento, D.B., Saito, S., Sandoval Gutierrez, M.I., Screaton, E.J., Smith-Duque, C.E., Solomon, E.A., Straub, S.M., Tanikawa, W., Torres, M.E., Uchimura, H., Vannucchi, P., Yamamoto, Y., Yan, Q., and Zhao, X., 2013d. Methods. *In* Harris, R.N., Sakaguchi, A., Petronotis, K., and the Expedition 344 Scientists, *Proceedings of the Integrated Ocean Drilling Program,* 344: College Station, TX (Integrated Ocean Drilling Program). **https://doi.org/10.2204/iodp.proc.344.102.2013**

Harris, R.N., Sakaguchi, A., Petronotis, K., Baxter, A.T., Berg, R., Burkett, A., Charpentier, D., Choi, J., Diz Ferreiro, P., Hamahashi, M., Hashimoto, Y., Heydolph, K., Jovane, L., Kastner, M., Kurz, W., Kutterolf, S.O., Li, Y., Malinverno, A., Martin, K.M., Millan, C., Nascimento, D.B., Saito, S., Sandoval Gutierrez, M.I., Screaton, E.J., Smith-Duque, C.E., Solomon, E.A., Straub, S.M., Tanikawa, W., Torres, M.E., Uchimura, H., Vannucchi, P., Yamamoto, Y., Yan, Q., and Zhao, X., 2013e. Upper slope Site U1413. *In* Harris, R.N., Sakaguchi, A., Petronotis, K., and the Expedition 344 Scientists, *Proceedings of the Integrated Ocean Drilling Program,* 344: College Station, TX (Integrated Ocean Drilling Program). **https://doi.org/10.2204/iodp.proc.344.107.2013**

Manheim, F.T., and Sayles, F.L., 1974. Composition and origin of interstitial waters of marine sediments, based on deep sea drill cores. *In* Goldberg, E.D. (Ed.), *The Sea* (Volume 5): *Marine Chemistry: The Sedimentary Cycle:* New York (Wiley), 527–568.

Morris, J.D., Villinger, H.W., Klaus, A., et al., 2003. *Proceedings of the Ocean Drilling Program, Initial Reports,* 205: College Station, TX (Ocean Drilling Program). **https://doi.org/10.2973/odp.proc.ir.205.2003**

Perry, E., and Hower, J., 1970. Burial diagenesis in Gulf Coast pelitic sediments. *Clays and Clay Minerals,* 18:165–177. **https://doi.org/10.1346/CCMN.1970.0180306**

Ranero, C.R., and von Huene, R., 2000. Subduction erosion along the Middle America convergent margin. *Nature,* 404(6779):748–752. **https://doi.org/10.1038/35008046**

Ranero, C.R., von Huene, R., Flueh, E., Duarte, M., Baca, D., and McIntosh, K., 2000. A cross section of the convergent Pacific margin of Nicaragua. *Tectonics,* 19(2):335–357. **https://doi.org/10.1029/1999TC900045**

Ross, N., Torres, M.E., Haley, B.A., Solomon, E.A., and Kastner, M., 2015. Data report: strontium isotope analyses of pore fluids from the CRISP-A transect drilled during Expeditions 334 and 344. *In* Harris, R.N., Sakaguchi, A., Petronotis, K., and the Expedition 344 Scientists, *Proceedings of the Integrated Ocean Drilling Program,* 344: Tokyo (Integrated Ocean Drilling Program Management

International, Inc.). https://doi.org/10.2204/iodp.proc.344.201.2015

Silver, E., Fisher, A., Saffer, D., Kastner, M., Morris, J., and McIntosh, K., 2000. Fluid flow paths in the Middle America Trench and Costa Rica margin. *Geology,* 28(8):679–682. https://doi.org/10.1130/0091-7613(2000)28<679:FFPITM>2.0.CO;2

Vannucchi, P., Galeotti, S., Clift, P.D., Ranero, C.R., and von Huene, R., 2004. Long-term subduction-erosion along the Guatemalan margin of the Middle America Trench. *Geology*, 32(7):617–620. https://doi.org/10.1130/G20422.1

Initial receipt: 7 March 2017
Acceptance: 10 August 2017
Publication: 26 September 2017
MS 344-207

Figure F1. A. Location map of sites drilled during IODP CRISP program. **B.** Location of Sites U1381–U1380 drilled during Expedition 344 along the A–A′ transect from the incoming plate to the upper slope. Sites U1381 and U1414 were drilled on the incoming plate. **C.** Schematic transect showing locations of sites along the A–A′ transect and indicating projected locations for Sites U1413 and U1414 (Expedition 334 Scientists, 2012).

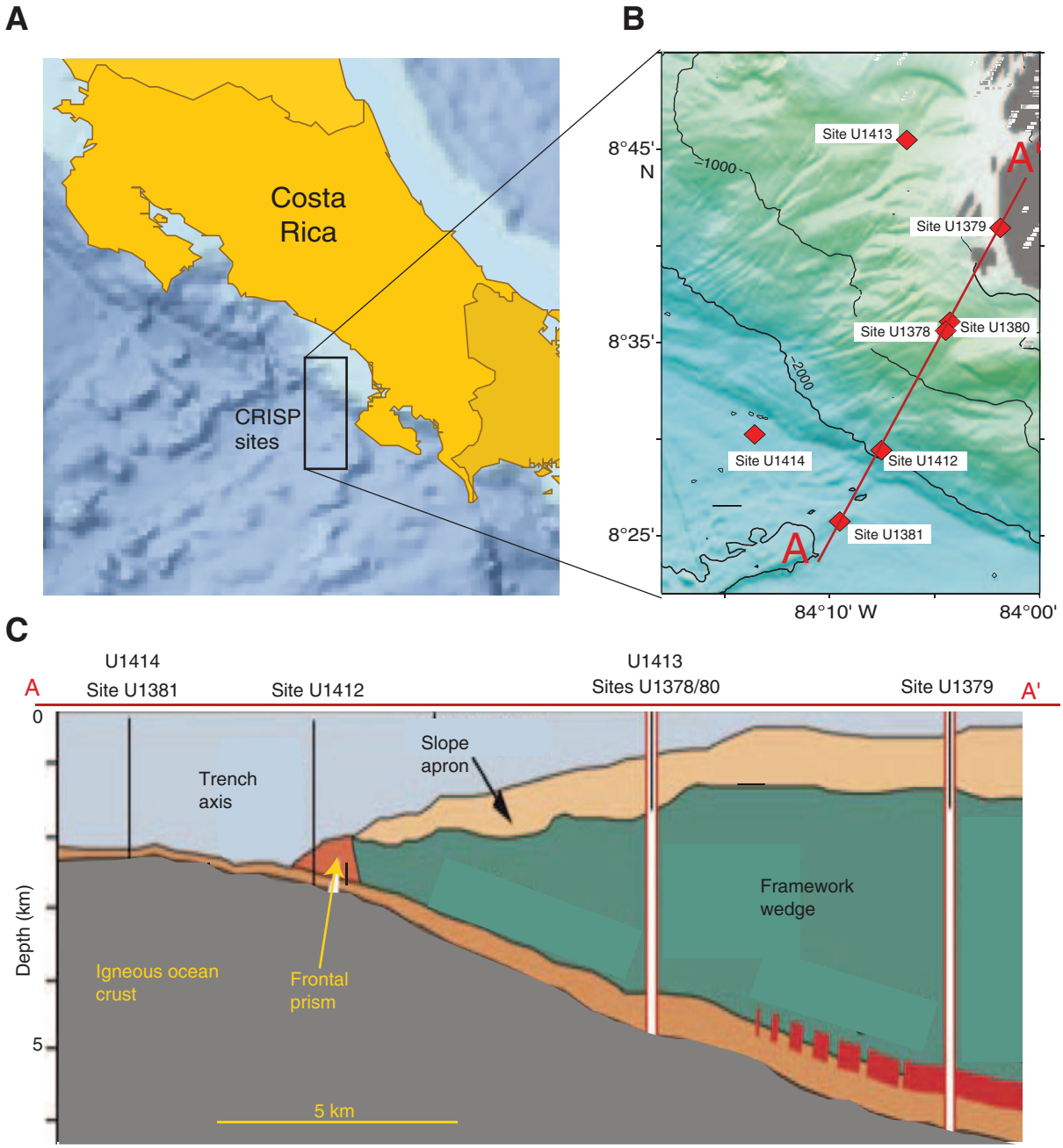

Figure F2. A. Concentration-depth profiles normalized to Cl for K, Rb, and Cs in pore fluids from Site U1380. **B.** Mixing diagrams for Site U1380 pore fluids.

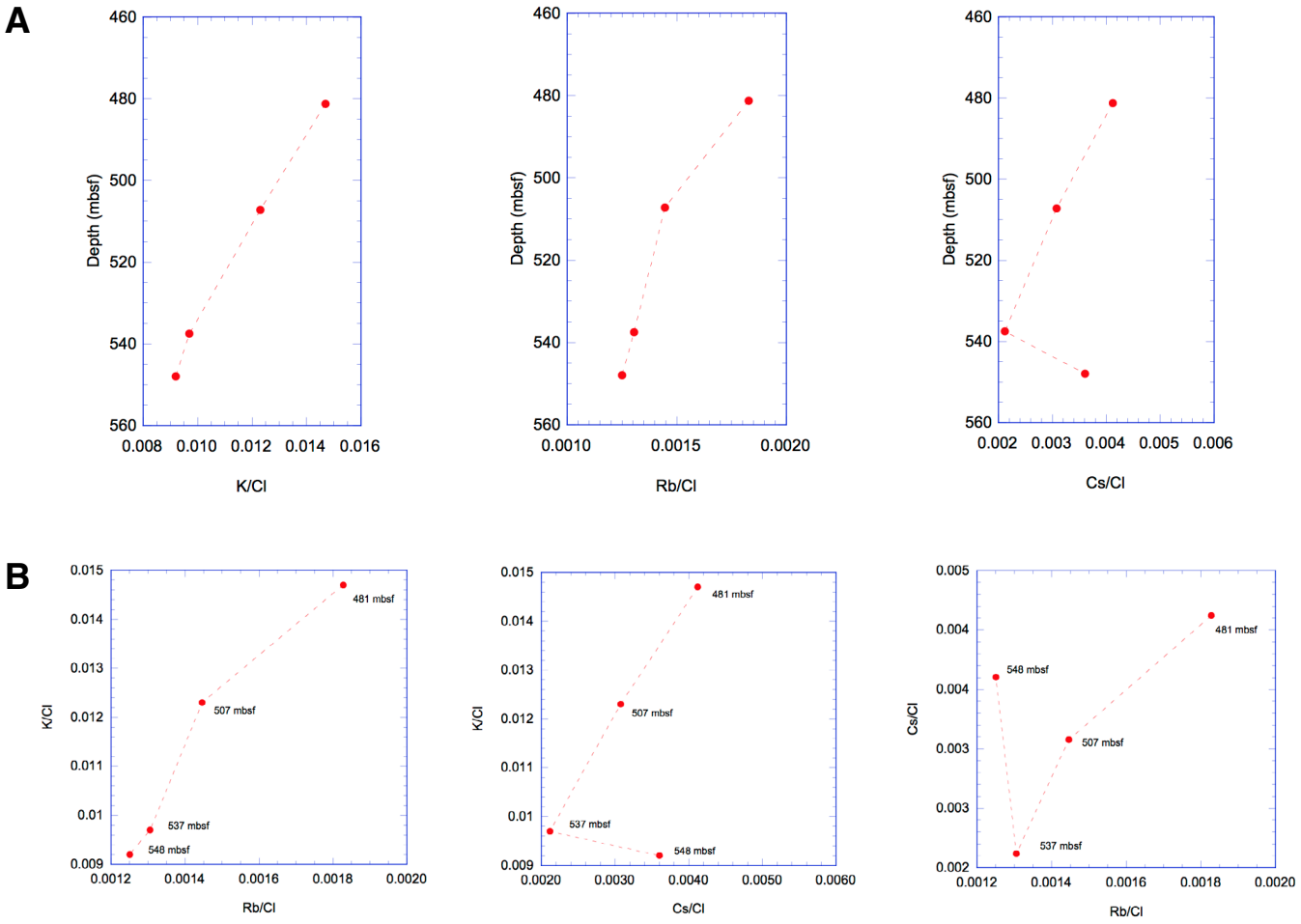

Figure F3. A. Concentration-depth profiles normalized to Cl for K, Rb, and Cs in pore fluids from Site U1413. **B.** Mixing diagrams for Site U1413 pore fluids.

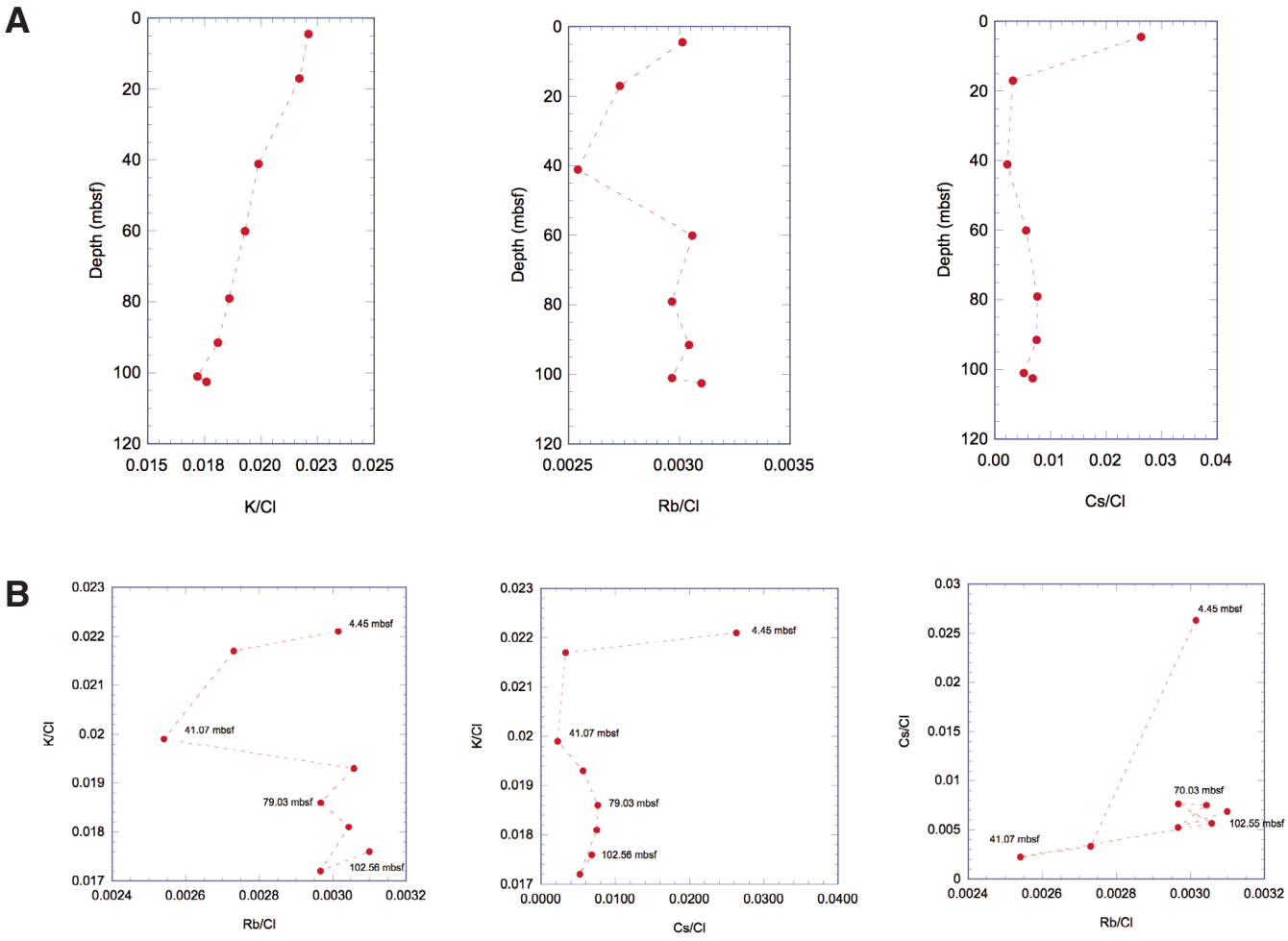

Figure F4. A. Concentration-depth profiles normalized to Cl for K, Rb, and Cs in pore fluids from Site U1412. **B.** Mixing diagrams for Site U1412 pore fluids.

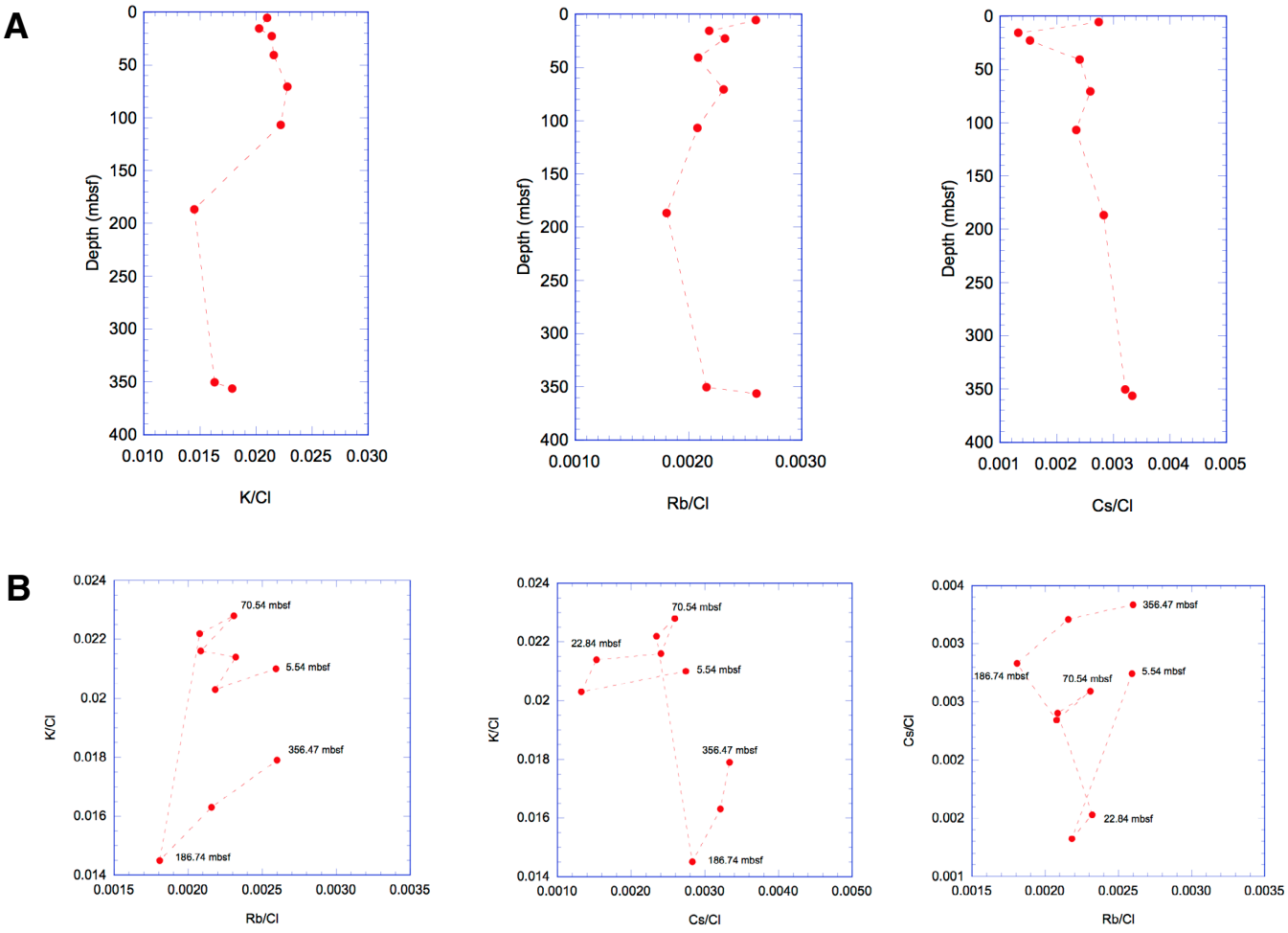

Figure F5. A. Concentration-depth profiles normalized to Cl for K, Rb, and Cs in pore fluids from Site U1381. **B.** Mixing diagrams for Site U1381 pore fluids.

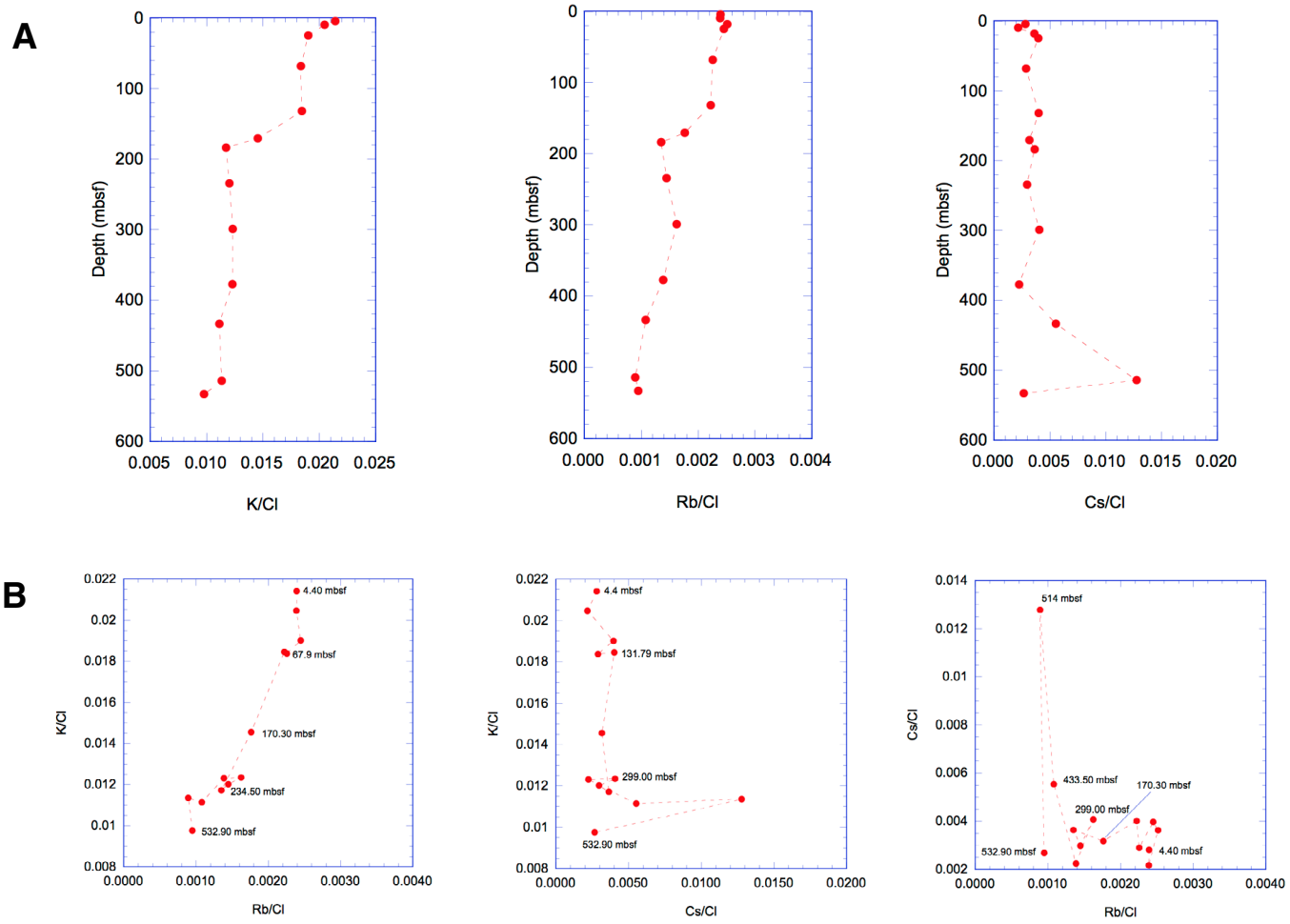

Figure F6. A. Concentration-depth profiles normalized to Cl for K, Rb, and Cs in pore fluids from Site U1414. **B.** Mixing diagrams for Site U1414 pore fluids.

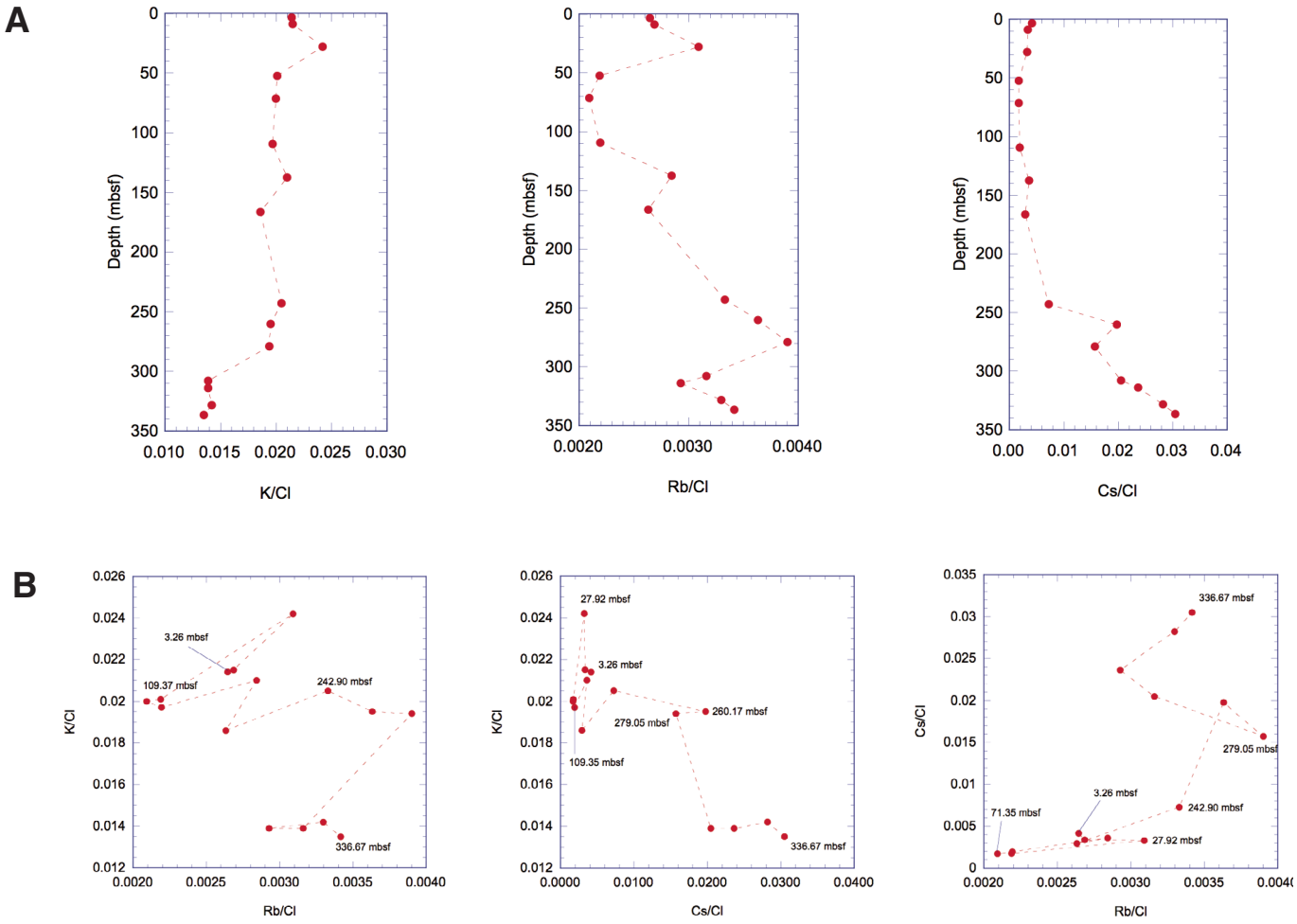

Table T1. Concentrations and Cl-normalized ratios of Cl, K, Rb, and Cs in pore fluid, Expedition 344.

Core, section, interval (cm)	Depth (mbsf)	Cl (mM)	K (mM)	K/Cl	Rb (μM)	Rb/Cl	Cs (nM)	Cs/Cl
344-U1380C-								
6R-3, 122–152	481.25	384	5.7	0.0147	0.70	0.0018	1.58	0.0041
9R-1, 102–132	507.22	401	4.9	0.0123	0.58	0.0014	1.23	0.0031
12R-2, 79–113	537.55	386	3.8	0.0097	0.50	0.0013	0.82	0.0021
13R-3, 50–80	548.02	381	3.5	0.0092	0.48	0.0013	1.37	0.0036
344-U1381C-								
1H-3, 140–150	4.45	556	12.3	0.0221	1.68	0.0030	14.63	0.0263
2H-6, 140–150	17.05	563	12.2	0.0217	1.54	0.0027	1.86	0.0033
5H-3, 140–150	41.07	567	11.3	0.0199	1.44	0.0025	1.27	0.0022
7H-3, 135–150	60.03	569	11.0	0.0193	1.74	0.0031	3.22	0.0057
9H-3, 135–150	79.03	570	10.6	0.0186	1.69	0.0030	4.36	0.0076
10H-5, 140–150	91.55	563	10.2	0.0181	1.71	0.0030	4.23	0.0075
11H-5, 140–150	101.05	561	9.7	0.0172	1.66	0.0030	2.94	0.0052
11H-6, 140–150	102.55	557	9.8	0.0176	1.73	0.0031	3.82	0.0069
344-U1412A-								
1H-4, 98–110	5.54	557	11.7	0.0210	1.44	0.0026	1.53	0.0027
2H-7, 106–118	15.38	562	11.4	0.0203	1.23	0.0022	0.74	0.0013
3H-5, 138–150	22.84	562	12.0	0.0214	1.31	0.0023	0.86	0.0015
5H-7, 133–150	40.50	565	12.2	0.0216	1.18	0.0021	1.36	0.0024
9H-6, 136–157	70.54	544	12.4	0.0228	1.26	0.0023	1.41	0.0026
15H-2, 93–115	106.75	563	12.5	0.0222	1.17	0.0021	1.32	0.0023
344-U1412B-								
6X-2, 99–125	186.74	556	8.05	0.0145	1.01	0.0018	1.57	0.0028
344–U1412C–								
7R-2, 96–112	350.31	560	9.13	0.0163	1.21	0.0022	1.80	0.0032
344-U1412D-								
2R-5, 106–131	356.47	552	9.86	0.0179	1.44	0.0026	1.84	0.0033
344-U1413A-								
2H-2, 138–150	9.50	552	11.3	0.0205	1.32	0.0024	1.20	0.0022
3H-6, 140–152	24.40	552	10.5	0.0190	1.35	0.0025	2.19	0.0040
8H-5, 136–156	67.90	555	10.2	0.0184	1.25	0.0023	1.61	0.0029
17H-2, 80–102	131.70	558	10.3	0.0185	1.24	0.0022	2.24	0.0040
22X-1, 56–85	170.30	560	8.15	0.0146	0.99	0.0018	1.78	0.0032
344-U1413B-								
1H-3, 140–150	4.40	551	11.80	0.0214	1.32	0.0024	1.55	0.0028
3H-2, 144–154	18.20	551	—	—	1.39	0.0025	2.00	0.0036
344–U1413C–								
2R-5, 53–83	183.90	551	6.46	0.0117	0.75	0.0014	2.01	0.0036
7R-6, 101–131	234.50	544	6.54	0.0120	0.79	0.0014	1.62	0.0030
14R-4, 16–61	299.00	543	6.70	0.0123	0.88	0.0016	2.21	0.0041
22R-4, 89–119	377.40	537	6.61	0.0123	0.75	0.0014	1.21	0.0022
28R-3, 88–123	433.50	530	5.91	0.0112	0.57	0.0011	2.94	0.0055
36R-5, 62–97	514.10	527	5.98	0.0113	0.47	0.0009	6.73	0.0128
38R-4, 117–152	532.90	542	5.29	0.0098	0.51	0.0010	1.45	0.0027
344-U1414A-								
2H-1, 131–141	3.26	557	11.9	0.0214	1.47	0.0026	2.32	0.0042
2H-5, 131–141	8.90	553	11.9	0.0215	1.49	0.0027	1.86	0.0034
4H-5, 132–142	27.92	466	11.3	0.0242	1.44	0.0031	1.52	0.0033
7H-2, 140–150	52.35	567	11.4	0.0201	1.24	0.0022	0.99	0.0017
9H-2, 140–150	71.35	571	11.4	0.0200	1.20	0.0021	0.98	0.0017
13H-2, 140–150	109.35	569	11.2	0.0197	1.25	0.0022	1.10	0.0019
16H-2, 110–120	137.55	566	11.9	0.0210	1.61	0.0028	2.03	0.0036
19H-3, 135–150	166.35	566	10.5	0.0186	1.49	0.0026	1.66	0.0029
27X-3, 130–150	242.90	567	11.6	0.0205	1.89	0.0033	4.12	0.0073
29X-2, 72–102	260.17	569	11.1	0.0195	2.07	0.0036	11.24	0.0198
31X-2, 65–100	279.05	567	11.0	0.0194	2.21	0.0039	8.91	0.0157
35X-1, 15–39	307.97	560	7.8	0.0139	1.77	0.0032	11.47	0.0205
36R-2, 67–92	314.01	561	7.8	0.0139	1.64	0.0029	13.27	0.0237
38R-2, 66–102	328.39	557	7.9	0.0142	1.84	0.0033	15.71	0.0282
39R-1, 80–94	336.67	555	7.5	0.0135	1.90	0.0034	16.93	0.0305